Monthly Notices
of the
ROYAL ASTRONOMICAL SOCIETY

MNRAS **435,** 1139–1146 (2013)
Advance Access publication 2013 August 30

doi:10.1093/mnras/stt1361

The long-wavelength view of GG Tau A: rocks in the ring world

Anna M. M. Scaife★

Department of Physics & Astronomy, University of Southampton, Highfield, Southampton SO17 1BJ, UK

Accepted 2013 July 18. Received 2013 July 16; in original form 2013 June 18

ABSTRACT

We present the first detection of GG Tau A at centimetre wavelengths, made with the Arcminute Microkelvin Imager Large Array at a frequency of 16 GHz ($\lambda = 1.8$ cm). The source is detected at $>6\,\sigma_{\rm rms}$ with an integrated flux density of $S_{16\,\rm GHz} = 249 \pm 45$ μJy. We use these new centimetre-wave data, in conjunction with additional measurements compiled from the literature, to investigate the long-wavelength tail of the dust emission from this unusual protoplanetary system. We use an MCMC-based method to determine maximum likelihood parameters for a simple parametric spectral model and consider the opacity and mass of the dust contributing to the microwave emission. We derive a dust mass of $M_{\rm d} \approx 0.1\,{\rm M}_{\odot}$, constrain the dimensions of the emitting region and find that the opacity index at $\lambda > 7$ mm is less than unity, implying a contribution to the dust population from grains exceeding ≈4 cm in size. We suggest that this indicates coagulation within the GG Tau A system has proceeded to the point where dust grains have grown to the size of small rocks with dimensions of a few centimetres. Considering the relatively young age of the GG Tau association in combination with the low derived disc mass, we suggest that this system may provide a useful test case for rapid core accretion planet formation models.

Key words: radiation mechanisms: general – stars: formation – ISM: clouds – ISM: general.

1 INTRODUCTION

The evolution of protoplanetary discs is crucial for distinguishing between different models of planet formation, and the long-wavelength emission from such discs is the key to understanding this evolution. A number of theoretical models for planet formation within circumstellar discs have been proposed: the formation of gas giants by core accretion and atmospheric accumulation (Pollack et al. 1996; Hubickyj, Bodenheimer & Lissauer 2005) is known to suffer from time-scale difficulties, although these can be alleviated by the extended models such as that of Alibert et al. (2005), who build on the standard core accretion models to provide a more rapid method of planet formation; alternatively, the theory of planet formation by gravitational instability mechanisms (Boss 1992, 1997; Rice, Lodato & Armitage 2005) is proposed, although this method has been noted to require protoplanetary disc masses generally in excess of those currently measured from sub-mm data to proceed successfully.

The second of these issues, that of missing mass, is exacerbated by an inexact understanding of the evolution of the dust emissivity, κ_ν, in these objects. Disc masses derived from sub-mm and centimetre flux densities are critically sensitive to the value of this parameter, with $M_{\rm d} \propto \kappa_\nu^{-1}$. An increase in the emissivity results in a decrease in the derived mass, and vice versa. Emissivity is a function of grain size and composition in the disc and, although it can be modelled theoretically, observationally determining its value and behaviour as a function of frequency is not trivial.

The effect of such multiplicity is a further issue which has been suggested to influence planet formation. It has been found that approximately a quarter of known extrasolar planets are located in binary or polystellar systems (e.g. Mugrauer & Neuhäuser 2009) and that this bias is generally considered to be due to the increased dynamical complexity of such systems which results in their inner regions being swept clear of material, allowing gas to flow through the gap and influence the mass gain of gas giant planets (Ayliffe & Bate 2010).

Determining the dust characteristics of the protoplanetary discs around young stars, whether in multiple systems or otherwise, is a complicated process. At submillimetre wavelengths, it is complicated by opacity effects as well as contamination by envelope- rather than disc-dominated emission at shorter wavelengths. At microwave frequencies, the emission from discs is thought to be largely optically thin, avoiding the former as well as the latter of these issues. However, the emission is significantly fainter than at sub-mm frequencies, and furthermore, it can be contaminated by additional radio emission from ionized gas in the vicinity of these objects (e.g. Owen, Scaife & Ercolano 2013).

Radio frequency measurements of discs provide a useful tool as the emission is expected to be optically thin at such long

★ E-mail: a.scaife@soton.ac.uk

wavelengths. In addition, in the Rayleigh–Jeans region ($h\nu \ll k_B T_d$), the opacity of the thermal emission from dust grains can be well approximated by a power law, $\kappa_\nu \propto \nu^\beta$. This index β can be related to the spectral index of flux density measurements, here defined as $S_\nu \propto \nu^\alpha$, as $\beta \simeq (1 + \Delta) \times (\alpha - 2)$, where Δ is the ratio of optically thick to optically thin emission (Beckwith et al. 1990). In the sub-mm region, 350 μm to 1.3 mm, this has been determined to have an average value $\Delta \simeq 0.2$ (Rodmann et al. 2006; Lommen et al. 2007); however, at much longer cm wavelengths $\Delta \to 0$, as the emission is entirely optically thin, and consequently, the largest grain sizes can be determined directly from a measure of the radio spectral index.

In spite of these advantages, there are also a number of disadvantages in observing discs at longer wavelengths. First, the emission is fainter due to the spectrum falling off steeply at lower frequencies. Secondly, there is confusion at longer wavelengths from the additional radio emission often associated with protostellar systems. Although higher resolution imaging offers significant advantages in this regard, separating residual radio emission from the dust emission still requires a careful disentangling of spectral components (see e.g. Melis et al. 2011). It has been shown (AMI Consortium: Scaife et al. 2012) that considering radio and dust components separately can give substantially different values for both the spectral slope of each component, important for determining opacity indices, as well as the normalization of each component, important for determining disc mass. Degeneracies between different parameters, increased in the case of lack of data or unfavourable spectral combinations, may be a limiting factor in the accuracy with which such parameters can be determined.

In this paper, we examine the long-wavelength emission from the well-known GG Tau A disc/ring system, extending the SED to centimetre wavelengths; we briefly describe this system in Section 2. In Section 3, we describe the new observations presented here and the data reduction method; in Section 4, we describe our SED-fitting procedure and present the results of those fits; in Section 5, we discuss the implications of these results and in Section 6, we draw our conclusions.

2 GG Tau A

GG Tau is a quadruple system (Leinert et al. 1991) within the Taurus molecular cloud (assumed distance 140 pc). It consists of a pair of binary systems, denoted A and B. GG Tau A, the subject of this work, is classified as a classical T Tauri star (CTTS) and is itself a close binary system with a separation of 35 au. This binary pair is surrounded by a circumbinary disc (Dutrey, Guilloteau & Simon 1994; Guilloteau, Dutrey & Simon 1999), which itself hosts a dense inner 'ring' (Piétu et al. 2011) of material with a width of only 50 au, which has led to its nickname of 'the ring world' (Guilloteau et al. 1999). The inner ∼150 au around the binary itself has been swept clear through the tidal interaction of the constituent stellar pair, although filamentary 'streamers' of material have been observed to extend from the inner edge of the outer circumbinary ring across this gap towards the central binary system and its inner circumstellar disc (McCabe, Duchêne & Ghez 2002; Krist et al. 2005; Piétu et al. 2011).

In the centimetre-wave regime, Bieging, Cohen & Schwartz (1984) previously observed the GG Tau system at 2 and 6 cm, but with a 3σ detection limit of 0.7 mJy beam^{-1} only GG Tau/N was detected in their data. Subsequently, the longest wavelength measurement of GG Tau was made at 7 mm by Rodmann et al. 2006, who detected extended emission at a resolution of 1.5 arcsec, but did not investigate the source further. Simon & Guilloteau (1992), observing the system at 2.6 mm, noted that the mass of the system, assuming completely optically thin emission from a uniform dust disc, would be 0.15 $M_\odot$. For this estimate, they assumed an isothermal disc, with a temperature of 15 K. Using temperature estimates from ^{13}CO data, resulting in $T(300\,\mathrm{au}) = 20$ K and modelling the resolved sub-mm data, the dust mass in the disc+ring system was found to be 0.12 $M_\odot$ (Guilloteau et al. 1999) whilst the mass of the ring alone was found to be 0.09 $M_\odot$ (Piétu et al. 2011). Both estimates were somewhat smaller than that of Ohashi et al. (1991), who derived a dust mass for the disc+ring system of 0.16 $M_\odot$. This discrepancy may be explained by the surface density assumed by Ohashi et al. (1991) which is approximately a factor of 1.6 higher than that used by the previously listed estimates. Allowing for differences in assumed physical characteristics, the range of dust mass estimates for GG Tau A is less than a factor of 2. Compared to the dynamical mass of the system (Guilloteau et al. 1999), the dust is approximately 10 per cent as massive.

3 OBSERVATIONS AND IMAGING

Arcminute Microkelvin Imager (AMI) comprises two synthesis arrays, one of ten 3.7 m antennas (SA) and another of eight 13 m antennas (LA), both sited at the Mullard Radio Astronomy Observatory at Lord's Bridge, Cambridge (AMI Consortium: Zwart et al. 2008). The telescope observes in the band 13.5–17.9 GHz with eight 0.75 GHz bandwidth channels. In practice, the two lowest frequency channels (1 and 2) are not generally used due to a lower response in this frequency range and interference from geostationary satellites. The data in this paper were taken with the AMI Large Array (AMI-LA).

Observations of GG Tau were made with the AMI-LA during 2011 August. AMI-LA data reduction is performed using the local software tool REDUCE. This applies both automatic and manual flags for interference, shadowing and hardware errors; Fourier transforms the correlator data to synthesize frequency channels; and performs phase and amplitude calibrations before output to disc in *uv* FITS format suitable for imaging in AIPS.[1] Flux (primary) calibration is performed using short observations of 3C286, 3C48 and 3C147. We assume I+Q flux densities for these sources in the AMI-LA channels consistent with the updated Very Large Array (VLA) calibration scale (Perley & Butler 2013). Since the AMI-LA measures I+Q, these flux densities include corrections for the polarization of the calibrator sources. A correction is also made for the changing air mass over the observation. From other measurements, we find that the flux calibration is accurate to better than 5 per cent (AMI Consortium: Scaife et al. 2008; AMI Consortium: Hurley-Walker et al. 2009). Additional phase (secondary) calibration is done using interleaved observations of calibrators selected from the Jodrell Bank VLA Survey (JVAS; Patnaik et al. 1992). After calibration, the phase is generally stable at 5° for channels 4–7, and at 10° for channels 3 and 8. The full width at half-maximum (FWHM) of the primary beam of the AMI-LA is ≈6 arcmin at 16 GHz. Due to their superior phase stability, only channels 4–7 were used for this work, resulting in an effective total bandwidth of 3 GHz and a central frequency of 15.7 GHz, referred to in this work as 16 GHz.

Reduced data were imaged using the AIPS data package. CLEAN deconvolution was performed using the task IMAGR which applies a differential primary beam correction to the individual frequency

[1] http://www.aips.nrao.edu/

channels to produce the combined frequency image. Due to the low declination of this sample, uniform visibility weighting was used to improve the AMI-LA point spread function. The AMI-LA is sensitive to angular scales from ≈0.5–6 arcmin, although this varies as a function of declination, hour angle coverage and data flagging.

In what follows, we use the convention: $S_\nu \propto \nu^\alpha$, where S_ν is flux density (rather than flux, $F_\nu = \nu S_\nu$), ν is frequency and α is the spectral index. All errors quoted are 1σ.

3.1 Separation of sources

GG Tau A is closely separated from GG Tau/N, which is widely thought to be an extragalactic radio source. The AMI-LA data towards GG Tau are dominated by GG Tau/N, with the peak of the 1.8 cm emission closely associated with the position of this radio source; an extension to the south can be seen in the direction of GG Tau A, see Fig. 1(a). We separate these sources by subtracting a point source located at the position of GG Tau/N directly from the visibilities. This subtraction assumes a flux density equivalent to the peak flux density in the AMI-LA map and therefore a negligible contribution at this location from GG Tau A. The subtracted data reveal a point source at J $04^{\rm h}32^{\rm m}30\overset{\rm s}{.}7 + 17^\circ31'35''$, see Fig. 1(b).

This point source is detected at $>6\sigma_{\rm rms}$ with a flux density of $S_{1.8\,\rm cm} = 249 \pm 45\,\mu$Jy. The error on this flux density includes an increased uncertainty on the absolute calibration to a level of 10 per cent to account for additional offsets which may be introduced by the subtraction of GG Tau/N as well as a contribution from the thermal noise. The error is given as the quadrature sum of these quantities, $\sigma = \sqrt{(0.1\,S_{1.8\,\rm cm})^2 + \sigma_{\rm rms}^2}$. The synthesized beam of the AMI-LA towards GG Tau for these data is $\Omega = 44 \times 25$ arcsec, resulting in a positional accuracy for the AMI-LA centroid at an effective signal-to-noise ratio of 5.5σ of ≈7 arcsec. Consequently, we identify this point source with GG Tau A as the radio peak is consistent with the infrared position of GG Tau A to $\approx 1\sigma$. The infrared position of GG Tau A is indicated by a cross in Fig. 1(b).

3.2 Expected contamination by extragalactic radio sources

At 16 GHz, we expect a certain number of extragalactic radio sources to be detected within the AMI-LA primary beam. We quantify this number using the 15 GHz source counts model from de Zotti et al. (2005) scaled to the 10C survey source counts (Davies et al. 2011). The rms noise in our data set is 38 μJy beam^{-1}, and from this model we predict that we should see $\simeq 1$ radio source within a 6 arcmin FWHM primary beam above a 5σ flux density of 190 μJy. Our results are compatible with this prediction as GG Tau/N is classified as an extragalactic source.

4 BLACKBODY SPECTRUM

The long-wavelength SED of CTTSs is expected to be dominated by the thermal dust contribution from the circumstellar disc. This contribution is generally considered to be well described by a modified blackbody spectrum,

$$S_\nu \propto \nu^\beta B_\nu(T_{\rm d}), \tag{1}$$

where $B_\nu(T_{\rm d})$ is the Planck function at a temperature $T_{\rm d}$ and β is the opacity index such that the dust opacity κ_ν can be described as $\kappa_\nu = \kappa_0(\nu/\nu_0)^\beta$.

In the simplest interpretation, for thermal dust emission the flux density at a given frequency is related to the disc mass by

$$M_{\rm d} = \frac{S_\nu \Psi d^2}{\kappa_\nu B_\nu(T_{\rm d})}, \tag{2}$$

where Ψ is the dust-to-gas ratio, κ_ν is the opacity at frequency ν and $B_\nu(T_{\rm d})$ is the value of the Planck function at frequency ν for a dust temperature $T_{\rm d}$. We use the dust opacity, $\kappa_\nu = 0.9(\nu/90.9\,{\rm GHz})^\beta$ cm^2 g^{-1} (Lommen et al. 2007).

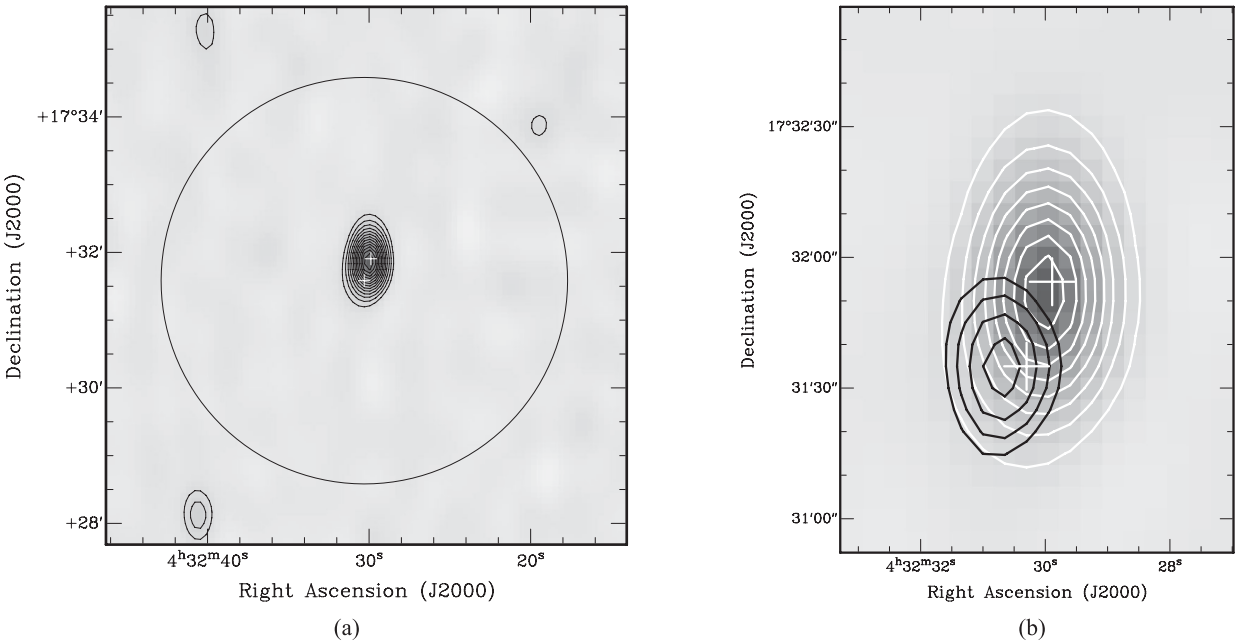

Figure 1. GG Tau A. (a) Grey-scale and contours show original data from the AMI-LA towards GG Tau A with linear contours from 5σ. The AMI-LA primary beam is indicated by a grey circle. (b) Grey-scale and white contours show original data from the AMI-LA towards GG Tau A at 5, 10, 20, 40σ, etc. The black contours show *uv*-subtracted data, see the text for details, at 3, 4, 5 and 6σ. In both maps, white crosses mark the positions of GG Tau/N to the north and GG Tau A to the south.

Table 1. Flux densities for GG Tau A from this work and compiled from the literature. Column 1 lists the frequency of the measurement, column 2 lists the flux density in mJy and column 3 lists the reference for each measurement.

ν (GHz)	S_ν (mJy)	Ref.
16.1	0.249 ± 0.045	This work
43.0	3.24 ± 0.42	Rodmann et al. (2006)
88.2	38 ± 2	Guilloteau et al. (1999)
98.0	41 ± 4.1	Ohashi et al. (1991)
110.0	82 ± 8.2	Koerner, Sargent & Beckwith (1993)
111.1	85 ± 5	Guilloteau et al. (1999)
115.3	96 ± 9.6	Kawabe et al. (1993)
116.3	90 ± 9.0	Simon & Guilloteau (1992)
214.3	604 ± 8	Guilloteau et al. (1999)
220.0	615 ± 61.5	Koerner et al. (1993)
225.0	557 ± 3	Harris et al. (2012)
230.0	593 ± 53	Beckwith et al. (1990)
230.0	593 ± 59	Andrews & Williams (2005)
272.0	800 ± 80	Beckwith & Sargent (1991)
353.0	1250 ± 125	Beckwith & Sargent (1991)
353.0	1255 ± 125.5	McCabe et al. (2006)
3000.0	5160 ± 520	IPAC (1986)
5000.0	3030 ± 303	IPAC (1986)
12 000.0	1360 ± 140	Cutri et al. (2012)
12 000.0	1650 ± 165	IPAC (1986)
25 000.0	736 ± 80	Cutri et al. (2012)
25 000.0	1270 ± 130	IPAC (1986)

Consequently, the modified blackbody spectrum of a given object can be normalized at a frequency ν_0 by a given disc mass, M_d, such that

$$S_\nu = \frac{M_\mathrm{d}}{\Psi d^2} \kappa_0 (\nu/\nu_0)^\beta B_\nu(T_\mathrm{d}). \quad (3)$$

In order to fit an SED to GG Tau A, we compile a set of data at different frequencies from the literature. These data are listed in Table 1 and shown in Fig. 2. These data are selected to only include measurements in which the disc and ring are expected to be spatially unresolved, i.e. the disc has not been resolved out as is the case in (e.g.) Piétu et al. (2011). We also restrict this compilation to that region of the spectrum which is expected to be dominated by the thermal emission from the disc and ring, limiting our coverage to $\lambda > 10\,\mu$m. Where no error is stated on these archival measurements, we adopt a standard 10 per cent error on the flux density. We fit the function in equation (3) to these data with dust temperature, disc mass and opacity index as free parameters and using a normalizing frequency of $\nu_0 = 100\,$GHz. We use a metropolis hastings MCMC code to determine the maximum likelihood parameter values, which we find to be $T_{\mathrm{d,\,ML}} = 19.42 \pm 0.55\,$K, $M_{\mathrm{d,\,ML}} = 0.099 \pm 0.004\,\mathrm{M}_\odot$ and $\beta_\mathrm{ML} = 0.96 \pm 0.04$. The fitted model is shown in Fig. 2. As expected, there is a strong negative correlation between the opacity index and dust temperature, with a correlation coefficient of $p = -0.82$, as well as weaker correlations between disc mass and dust temperature ($p = -0.64$), and disc mass and opacity index ($p = 0.33$).

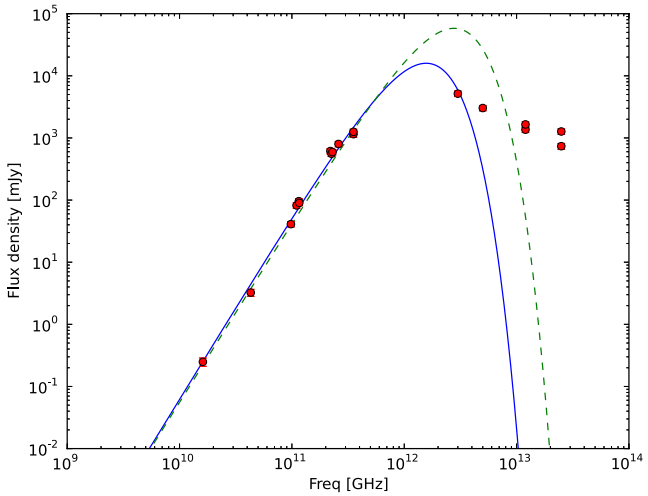

Figure 2. SED of GG Tau A. Flux density measurements from this work and compiled from the literature, see Table 1, are shown as data points with associated error bars. The maximum likelihood SED is shown as a solid line, see Section 4, and an SED with the dust temperature fixed at $T_\mathrm{d} = 35\,$K is shown as a dashed line, see Section 4 for details.

4.1 Disc mass and dust temperature

The disc mass recovered by fitting the GG Tau A SED is intermediate to the values recovered previously for the dense inner ring, $M_\mathrm{ring} = 0.09\,\mathrm{M}_\odot$ (Piétu et al. 2011), and the larger circumbinary disc–ring system, $M_\mathrm{system} = 0.12\,\mathrm{M}_\odot$ (Guilloteau et al. 1999). The dust temperature recovered from fitting the SED is relatively cold. Guilloteau et al. (1999) suggested that the temperature of the GG Tau A system dropped steeply with radial distance from the central object, resulting in a temperature of $T(R = 300\,\mathrm{au}) \approx 20\,$K. Since the single temperature assumed in equation (3) will be a mass-weighted average temperature for the combined emission, this suggests that the mass of dust contributing to the centimetre-wave flux density is dominated by the colder dust population.

At smaller radial distances the dust temperature of the GG Tau A system has been modelled to be much higher, with $T(R = 50\,\mathrm{au}) \approx 35\,$K. An SED with a dust temperature fixed to this value is also fitted with the data set in Table 1. The best-fitting SED from this fitting is shown as a dashed line in Fig. 2, where it can be seen that it is inconsistent with the measured far-infrared shape of the GG Tau A SED.

4.2 Opacity index

Given the power-law approximation to the dust opacity as stated in Section 4, the opacity index, β, can be determined using the ratio of flux densities at two frequencies such that

$$\frac{S_{\nu_1}}{S_{\nu_2}} = \gamma \left(\frac{\nu_1}{\nu_2}\right)^{3+\beta}, \quad \text{where} \quad \gamma = \frac{\mathrm{e}^{h\nu_2/kT_\mathrm{d}} - 1}{\mathrm{e}^{h\nu_1/kT_\mathrm{d}} - 1} \quad (4)$$

and consequently

$$\beta = \frac{\ln\left(S_{\nu_1}/S_{\nu_2}\right) - \ln\gamma}{\ln\left(\nu_1/\nu_2\right)} - 3 \quad (5)$$

with an associated error

$$\sigma_\beta = \left|\frac{1}{\ln(\nu_1/\nu_2)}\right| \sqrt{\left(\frac{\sigma_{S_{\nu_1}}}{S_{\nu_1}}\right)^2 + \left(\frac{\sigma_{S_{\nu_2}}}{S_{\nu_2}}\right)^2}. \quad (6)$$

Fitting all of the data in Table 1 with a single modified blackbody results in an opacity index $\beta = 0.96 \pm 0.04$, see Section 4. However, the composite nature of the GG Tau A system, with its disc plus ring, suggests that although the data seem well modelled by a single modified blackbody, there may be multiple components

Table 2. Maximum likelihood parameter constraints from model fitting, see Section 4 for details.

Data range	M_d ($M_\odot$)	β	T_d (K)
Prior	[0, 1]	[0, 2]	[0, 50]
All data	0.099 ± 0.004	0.96 ± 0.04	19.42 ± 0.55
$\lambda > 3$ mm	0.096 ± 0.005	1.07 ± 0.10	20[a]
$\lambda \geq 7$ mm	–	0.69 ± 0.26	–

[a] Fixed parameter.

contributing to the SED. Specifically, we would expect the longest wavelength emission to have a larger relative contribution from that dust population which has the largest grain sizes and hence a flattened spectrum. Consequently, fixing the dust temperature at 20 K, we refit only those data with $\nu < 100$ GHz. This fit results in very similar parameter constraints: $M_{\rm disc} = 0.096 \pm 0.005\,{\rm M}_\odot$ and $\beta = 1.07 \pm 0.10$. However, the allowed range of parameter space, compared with the full SED fit, allows a range of much smaller disc masses and flatter values of β. Furthermore, using the expressions in equations (5) and (6), the opacity index from 1.8 cm to 7 mm is $\beta_{1.8\,{\rm cm}}^{7\,{\rm mm}} = 0.64 \pm 0.24$, which implies a much flatter spectrum. This suggests that if there is a separate contribution from a larger dust-grain population, it only appears at wavelengths longer than ∼7 mm. These results are summarized in Table 2.

5 DISCUSSION

5.1 Optically thick fraction

In the Rayleigh–Jeans region, the thermal emission from dust grains can be well approximated by a power law with $S_\nu \propto \nu^\alpha$. The spectral index α is related to the dust opacity index β as

$$\beta \simeq (1 + \Delta) \times (\alpha - 2), \tag{7}$$

where Δ is the ratio of optically thick to optically thin emission (Beckwith et al. 1990). In the sub-mm region, 350 μm to 1.3 mm, this has been determined to have an average value $\Delta \simeq 0.2$ (Rodmann et al. 2006; Lommen et al. 2007).

Although at longer wavelengths Δ is expected to tend to zero, the exact value is a function of the column density, which may be very high in the inner regions of the disc causing the opacity to be non-negligible even at centimetre wavelengths. It may be calculated using the radial power-law indices of the disc surface density and temperature, denoted p and q, respectively, as

$$\Delta \approx -p \times [(2 - q)\ln\{(1 - p/2)\bar{\tau}\}]^{-1}, \tag{8}$$

where $\bar{\tau}$ is the average disc opacity at the measurement frequency, defined as

$$\bar{\tau} \equiv \frac{\kappa_\nu M_{\rm d}}{\Psi \cos\theta \pi R_{\rm d}^2} \tag{9}$$

(e.g. Beckwith et al. 1990), where θ is the inclination of the disc to the line of sight ($\theta = 0^\circ$ for a face on disc) and $R_{\rm d}$ is the outer radius of the disc.

The surface density of discs is expected to decrease with radius, leading to positive values of p. A value of $p = 1.5$ is typically assumed (Beckwith et al. 1990; Rodmann et al. 2006), and we also adopt this value here. The power-law index of the radial temperature, defined such that $T(r) = T_0(r/r_0)^{-q}$, is uniquely determined from the infrared spectral index, $\alpha_{\rm IR}$, calculated at wavelengths where the opacity is expected to be high, typically $\lambda < 100$ μm, such that $q = 2/(3 - \alpha_{\rm IR})$. Although we note that this power-law approximation breaks down at shorter wavelengths where reprocessing of stellar photons will modify the value of q. Using measurements from the *IRAS* and *WISE* catalogues, see Table 1, we find that $q = 0.5$–0.6 for GG Tau A. However, we note that the more complex modelling of this system by Guilloteau et al. (1999) found a value of $q = 0.9 \pm 0.1$, implying a steeper radial temperature power law.

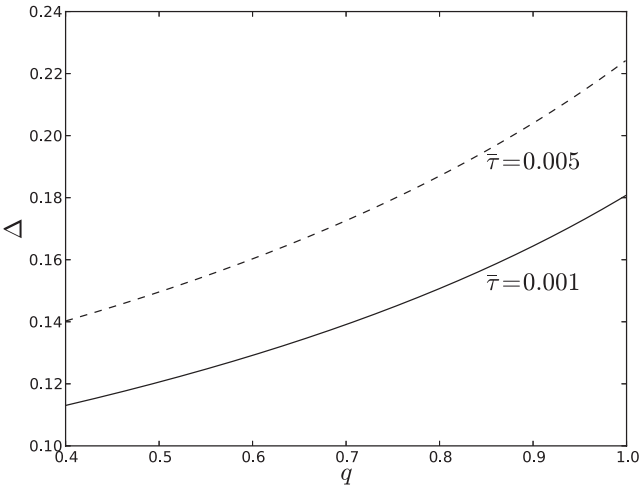

Figure 3. Fraction of optically thick to optically thin emission, Δ, at $\lambda = 2$ cm as a function of the radial temperature power-law index, q, for limiting values of the average disc opacity, $\bar{\tau}$, see Section 4.2 for details.

At millimetre wavelengths, Lommen et al. (2007) adopted a value of $\bar{\tau} = 0.02$ at 3.3 mm and Rodmann et al. (2006) adopted $\bar{\tau} = 0.01$ at 7 mm, consistent with the results of Beckwith et al. (1990). Consequently, at 1.8 cm, we expect that $\bar{\tau} \ll 0.01$. Extrapolating linearly from the millimetre values gives a value of $\bar{\tau} = 3.7 \times 10^{-3}$ at a wavelength of 1.8 cm. Since this is an inexactly determined value, we consider a range $0.001 \leq \bar{\tau} \leq 0.005$. Combining this with the adopted value of p, we find that $\Delta = 0.12$–0.15 for $q = 0.55$ and $\Delta = 0.16$–0.20 for $q = 0.9$. The general behaviour of Δ as a function of q and $\bar{\tau}$ is illustrated in Fig. 3.

Using data at 1.8 cm and 7 mm, we find a spectral index of $\alpha_{0.7}^{1.8} = 2.61 \pm 0.23$. The error on this index is a function not only of the precision with which the flux densities are measured at each frequency but also the bandwidth between those frequencies, with more closely separated frequencies necessarily resulting in larger errors on spectral index. We note that for the available data at 7 mm and 1.8 cm, the error on spectral index is an order of magnitude larger than the spread in the values of β produced by the uncertainty in Δ allowed by our range of $\bar{\tau}$ values. Using equation (7), we find $\beta = 0.69 \pm 0.26$. The indicative error on this value comes from propagating both the error on the spectral index as well as an error from treating the spread in allowed values of Δ as 1σ bounds on a central value. This value for β is consistent with that found from equations (5), see Section 4.2.

5.2 Grain-size distribution

The opacity index at a wavelength, λ, is expected to be related to the opacity index of the diffuse interstellar medium (ISM) as $\beta(\lambda) \approx (\chi - 3)\beta_{\rm ISM}$, where χ is the power-law index of the grain-size distribution such that $dn/da \propto a^{-\chi}$. Grain sizes a are limited in size to a maximum of $a \leq a_{\rm max}$. For the typically assumed MRN

power-law distribution (Mathis, Rumpl & Nordsieck 1977), where $\chi = 3.5$, an opacity index measured at a given wavelength, λ, with a value of $\beta(\lambda) \approx 1$ indicates $a_{\rm max} > \lambda$, and $\beta(\lambda) \leq 1$ corresponds to $a_{\rm max} > 3\lambda$ (Draine 2006). Although it has been shown through simulations that the growth of dust particles in protoplanetary discs may result in a flatter power-law size distribution with $\chi = 3$ (Tanaka, Himeno & Ida 2005), Draine (2006) argued that a power-law index of $\chi = 3.5$ was likely for protoplanetary environments where processes of fragmentation and coagulation were in competition to provide the grain-size distribution, and that the maximum grain size would be determined by the extent to which coagulation had progressed.

From these new data presented here, we find that β is consistent with unity into the centimetre regime implying that for $\chi = 3.5$, $a_{\rm max} > 2$ cm. However, the opacity index constrained from data at $\lambda > 7$ mm alone is less than unity. Taking the wavelength of measurement as the geometric mean of 7 mm and 1.8 cm suggests that $a_{\rm max} > 3\lambda \approx 4.2$ cm. Once again this is consistent with a grain-size distribution power-law index of $\chi = 3.5$; assuming $\beta_{\rm ISM} = 1.7$ (Finkbeiner, Davis & Schlegel 1999), the measured opacity index implies a power-law grain-size distribution with $\chi = 3.4 \pm 0.2$. This implies that coagulation within the GG Tau A system has proceeded to the point where dust grains have grown to size of small rocks with dimensions of a few centimetres.

5.3 Emitting region

By considering equation (9), we can use the disc mass calculated from the GG Tau A SED to calculate the emitting region by constraining its outer radius, $R_{\rm d}$. For a disc mass of $M_{\rm d} = 0.099 \pm 0.01\,{\rm M}_{\odot}$, see Section 4, and assuming $\theta = 37^{\circ}$ (Guilloteau et al. 1999; Piétu et al. 2011), a limiting $\bar{\tau} < 0.01$ implies an outer radius of $R_{\rm d} > 240$ au. For the proposed range of $\bar{\tau} = 0.001{-}0.005$ at $\lambda = 2$ cm, the corresponding range of $R_{\rm d}$ is shown in Fig. 4.

These values encompass the radial range allowed by the model of Guilloteau et al. (1999), who proposed that the GG Tau A system could be described by a dense ring of material with an outer radius of $R_{\rm ring} = 250 \pm 2$ au and a lower density disc with an outer radius of $R_{\rm disc} \approx 800$ au. The range of radii allowed by the mass and opacity

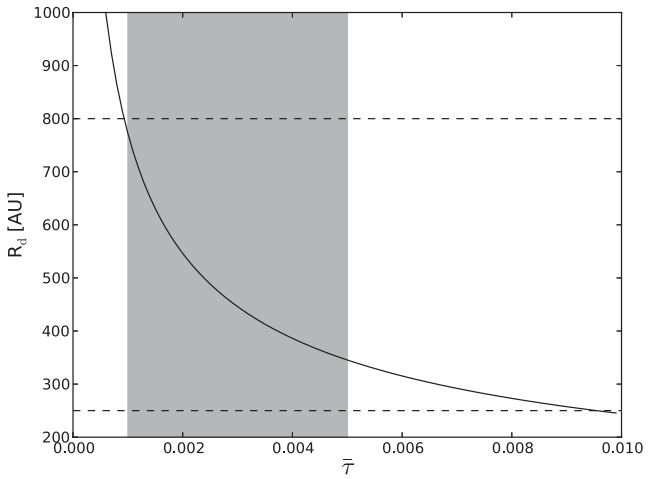

Figure 4. Outer radius of the emitting disc, $R_{\rm d}$, at 1.8 cm as a function of the average disc opacity, $\bar{\tau}$. The proposed range of $\bar{\tau}$ at 1.8 cm is indicated by the shaded area. The dashed lines indicate the proposed outer radius of the GG Tau A ring at 250 au and the outer radius of the GG Tau A disc at 800 au (Guilloteau et al. 1999).

constraints from the 1.8 cm data suggest that the emission we are seeing is consistent with a combined contribution from both the ring and the disc. This is consistent with the mass calculated from the 1.8 cm data being intermediate to that of the ring alone and the combined system. The value of the ring mass was previously calculated to be $M_{\rm ring} = 0.09\,{\rm M}_{\odot}$ (Piétu et al. 2011), whereas the mass of the ring+disc system was calculated as $M_{\rm system} = 0.12\,{\rm M}_{\odot}$ (Guilloteau et al. 1999).

5.4 Possible contamination from other radio emission mechanisms

At centimetre wavelengths, contamination from thermal bremsstrahlung or other radio emission mechanisms is a possibility for systems such as GG Tau A. Free–free emission from young stellar objects (YSOs) may arise as a consequence of shock ionization in molecular outflows (e.g. Curiel et al. 1989), although this is unlikely in the case of GG Tau A due to the absence of any detected molecular emission from a jet or an outflow. Molecular hydrogen has been detected in the regions interior to the GG Tau A ring (Beck et al. 2012); however, this rovibrational emission is thought to be associated with an accretion streamer, rather than shock excitation. Such emission may also be a result of stimulation by X-ray or UV flux from a central object, but in this case the distribution of the H_2 emission imaged at high resolution was found to be inconsistent with such a scenario (Beck et al. 2012). Such X-ray or UV flux can also give rise to free–free emission from photoionization of disc winds in CTTSs (Owen et al. 2013); however, in the case of GG Tau A, no X-ray counterpart is detectable ($L_{\rm X} < 2.5 \times 10^{29}$ erg s^{-1}; Neuhäuser et al. 1995) and photoionization due to UV flux is also unlikely as this is expected to result in an isothermal flow with temperatures of approximately 10^4 K. For GG Tau A, the $2{-}1\,{\rm S}(1)/1{-}0\,{\rm S}(1)$ line ratio indicates much lower temperatures of $\sim$1700 $\pm$ 100 K (Beck et al. 2012), inconsistent with this scenario.

Weak-line T Tauri stars (WTTSs) are expected to produce radio emission of a non-thermal nature due to magnetic activity in the stellar corona. This radio luminosity of such emission is tightly coupled to X-ray emission as a common energy reservoir is thought to fuel both the magnetic activity and heating of the surrounding gas giving rise to thermal bremsstrahlung in the X-ray regime (see Feigelson & Montmerle 1999 for a review). Such radio emission is expected to follow the 'Güdel–Benz relation' (Güdel & Benz 1993; Güdel 2002), often represented as the ratio $L_{\rm X}/L_{\rm rad} \sim 10^{15}$. Given the limits on X-ray luminosity from the *ROSAT* satellite (Neuhäuser et al. 1995), this relation would suggest a radio flux density of $S < 5\,\mu$Jy at 5−8 GHz for GG Tau A. Even assuming a flat spectral index to 16 GHz, this provides a negligible contribution to the measured flux density. CTTS systems are expected to be magnetically similar to WTTS, although non-thermal gyrosynchrotron emission produced close to the star is expected to suffer substantial absorption by disc and YSO winds, and therefore appear reduced. If this is indeed the case, the already negligible expected contribution from non-thermal emission to the 16 GHz flux density will be reduced even further.

5.5 Comparison to similar systems

Grain growth such as that seen here in the GG Tau A system is not unknown elsewhere. Perhaps the prototypical system for such spectral flattening at long wavelengths is TW Hya (Wilner et al. 2000), where 7 mm observations at high resolution reveal a disc, thought to be seen almost face on, with $\beta \approx 1$. However, at longer wavelengths, $\lambda = 3.5$ cm, a substantial excess of emission (confirmed as dust emission rather than free–free emission due to a non-detection

at 6 cm) is detected, which can only be explained by the presence of centimetre-size grains (Wilner et al. 2005).

The disc mass in the TW Hya system is similar to that derived here, $M_{\rm d} \approx 0.1\,{\rm M}_{\odot}$, neither high enough for the gravitational instability method of planet formation to occur (Boss 1998). Noting this, we consider the respective ages of the two systems. The TW Hya system is substantially older (5–10 Myr; Song, Zuckerman & Bessell 2003) than GG Tau A (∼1.5 Myr; White et al. 1999). This is important when considering the implications of grain growth and the potential of the system to form planetesimals via the core accretion model. The canonical time-scale for core accretion planet formation is 8 Myr (Pollack et al. 1996), nominally precluding planet formation in both the GG Tau A and TW Hya systems. However, Hubickyj et al. (2005) calculated that a reduction in dust opacity could reduce this time-scale to half, and, subsequently, the migration and disc evolution model of Alibert et al. (2005) demonstrated that in fact the formation time-scale could be reduced to as little as 1–3 Myr. Furthermore, this reduction in time-scale due to migration is not mutually exclusive with that due to dust opacity reduction, and the combination of effects would shorten formation times even further. These revised versions of the core accretion mechanism of planet formation suggest that planet formation is feasible even in systems as young as GG Tau A. Indeed, planet formation has been suggested for even younger systems still, such as in the case of HL Tau, a Class I object (10^5 yr; Greaves et al. 2008). Although in the case of HL Tau the disc mass was found to be high enough to allow the gravitational instability model of planet formation to operate. Once again the opacity index of the long-wavelength emission from HL Tau was suggestive of centimetre-size grains and in this case a surface density enhancement (4.5σ) was detected and proposed as a potential protoplanet.

6 CONCLUSIONS

We have detected the GG Tau A ring/disc system at a wavelength of $\lambda = 1.8$ cm. Using these new data in combination with archival data compiled from the literature, we have investigated the long-wavelength SED of the system with a number of results.

We propose that the detected flux is due to thermal dust emission from the GG Tau A system and that additional radio emission mechanisms contribute negligibly to the integrated flux density, if at all. We suggest that, although the centimetre-wave emission is dominated by the dense GG Tau A ring, the outer radius of the emission is larger than that of the ring alone and is therefore likely to encompass the complete ring/disc system. We find a dust mass for the GG Tau A combined ring/disc system of $M_{\rm d} = 0.099 \pm 0.004\,{\rm M}_{\odot}$.

We find that the opacity index of the GG Tau A long-wavelength emission is broadly consistent with unity, but there are indications that the spectrum flattens further at wavelengths longer than 7 mm. We suggest that this flattening of the spectrum implies a dust population with maximum grain sizes in excess of 4 cm and that this indicates coagulation of dust grains within the GG Tau A system into bodies more similar in size to small rocks than traditional dust.

With the indication of grain growth in the disc and considering the relatively young age of the GG Tau association (∼1.5 Myr) in combination with the low derived disc mass, we suggest that this may be a good system with which to test rapid planet formation models such as that of Alibert et al. (2005).

ACKNOWLEDGEMENTS

We thank the anonymous referee whose useful comments improved this paper. We thank the staff of Lord's Bridge Observatory for their invaluable assistance in the commissioning and operation of the Arcminute Microkelvin Imager. The AMI-LA is supported by Cambridge University and the STFC.

REFERENCES

Alibert Y., Mordasini C., Benz W., Winisdoerffer C., 2005, A&A, 434, 343
Andrews S. M., Williams J. P., 2005, ApJ, 631, 1134
Ayliffe B. A., Bate M. R., 2010, MNRAS, 408, 876
Beck T. L., Bary J. S., Dutrey A., Piétu V., Guilloteau S., Lubow S. H., Simon M., 2012, ApJ, 754, 72
Beckwith S. V. W., Sargent A. I., 1991, ApJ, 381, 250
Beckwith S. V. W., Sargent A. I., Chini R. S., Guesten R., 1990, AJ, 99, 924
Bieging J. H., Cohen M., Schwartz P. R., 1984, ApJ, 282, 699
Boss A. P., 1992 in McAlister H. A., Hartkopf W. I., eds, ASP Conf. Ser. Vol. 32, Complementary Approaches to Double and Multiple Star Research. Astron. Soc. Pac., San Francisco, p. 195
Boss A. P., 1996, ApJ, 469, 906
Boss A. P., 1998, ApJ, 503, 923
Curiel S., Rodriguez L. F., Bohigas J., Roth M., Canto J., Torrelles J. M., 1989, Astrophys. Lett. Commun., 27, 299
Cutri R. M. et al., 2012, VizieR On-line Data Catalog, 2311, 0
Davies M. L. et al., 2011, MNRAS, 415, 2708
de Zotti G., Ricci R., Mesa D., Silva L., Mazzotta P., Toffolatti L., González-Nuevo J., 2005, A&A, 431, 893
Draine B. T., 2006, ApJ, 636, 1114
Dutrey A., Guilloteau S., Simon M., 1994, A&A, 286, 149
Feigelson E. D., Montmerle T., 1999, ARA&A, 37, 363
Finkbeiner D. P., Davis M., Schlegel D. J., 1999, ApJ, 524, 867
Greaves J. S., Richards A. M. S., Rice W. K. M., Muxlow T. W. B., 2008, MNRAS, 391, L74
Güdel M., 2002, ARA&A, 40, 217
Guedel M., Benz A. O., 1993, ApJ, 407, L63
Guilloteau S., Dutrey A., Simon M., 1999, A&A, 348, 570
Harris R. J., Andrews S. M., Wilner D. J., Kraus A. L., 2012, ApJ, 751, 115
Helou G., Walker D. W., 1988, Infrared Astronomical satellite (IRAS) Catalogs and Atlases, NASA, Washington, Vol. 7, p. 1
Hubickyj O., Bodenheimer P., Lissauer J. J., 2005, Icarus, 179, 415
Hurley-Walker N. et al., 2009, MNRAS, 396, 365
Kawabe R., Ishiguro M., Omodaka T., Kitamura Y., Miyama S. M., 1993, ApJ, 404, L63
Koerner D. W., Sargent A. I., Beckwith S. V. W., 1993, ApJ, 408, L93
Krist J. E. et al., 2005, AJ, 130, 2778
Leinert C., Haas M., Mundt R., Richichi A., Zinnecker H., 1991, A&A, 250, 407
Lommen D. et al., 2007, A&A, 462, 211
Mathis J. S., Rumpl W., Nordsieck K. H., 1977, ApJ, 217, 425
McCabe C., Duchêne G., Ghez A. M., 2002, ApJ, 575, 974
McCabe C., Ghez A. M., Prato L., Duchêne G., Fisher R. S., Telesco C., 2006, ApJ, 636, 932
Melis C. et al., 2011, ApJ, 739, L7
Mugrauer M., Neuhäuser R., 2009, A&A, 494, 373
Neuhäuser R., Sterzik M. F., Schmitt J. H. M. M., Wichmann R., Krautter J., 1995, A&A, 297, 391
Ohashi N., Kawabe R., Ishiguro M., Hayashi M., 1991, AJ, 102, 2054
Owen J. E., Scaife A. M. M., Ercolano B., 2013, preprint (arXiv:1307.2240)
Patnaik A. R., Browne I. W. A., Wilkinson P. N., Wrobel J. M., 1992, MNRAS, 254, 655
Perley R. A., Butler B. J., 2013, ApJS, 204, 19
Piétu V., Gueth F., Hily-Blant P., Schuster K.-F., Pety J., 2011, A&A, 528, A81
Pollack J. B., Hubickyj O., Bodenheimer P., Lissauer J. J., Podolak M., Greenzweig Y., 1996, Icarus, 124, 62
Rice W. K. M., Lodato G., Armitage P. J., 2005, MNRAS, 364, L56
Rodmann J., Henning T., Chandler C. J., Mundy L. G., Wilner D. J., 2006, A&A, 446, 211
Scaife A. M. M. et al., 2008, MNRAS, 385, 809
Scaife A. M. M. et al., 2012, MNRAS, 420, 3334

Simon M., Guilloteau S., 1992, ApJ, 397, L47
Song I., Zuckerman B., Bessell M. S., 2003, ApJ, 599, 342
Tanaka H., Himeno Y., Ida S., 2005, ApJ, 625, 414
White R. J., Ghez A. M., Reid I. N., Schultz G., 1999, ApJ, 520, 811
Wilner D. J., Ho P. T. P., Kastner J. H., Rodríguez L. F., 2000, ApJ, 534, L101
Wilner D. J., D'Alessio P., Calvet N., Claussen M. J., Hartmann L., 2005, ApJ, 626, L109
Zwart J. T. L. et al., 2008, MNRAS, 391, 1545

This paper has been typeset from a TEX/LATEX file prepared by the author.